arXiv:1210.1991v1 [cond-mat.mtrl-sci] 6 Oct 2012

Toward an accurate modeling of x-ray magnetic circular dichroism in (Ge,Mn) compounds

Samuel Tardif,[1, 2, *] Andrey Titov,[1, 2, 3] Emmanuel Arras,[2] Ivetta Slipukhina,[2] El-Kébir Hlil,[1] Salia Cherifi,[4]
Yves Joly,[1] Mathieu Jamet,[2] André Barski,[2] Joël Cibert,[1] Erkin Kulatov,[3] Yurii A. Uspenskii,[5] and Pascal Pochet[2, †]
[1]*Institut Néel, CNRS-UJF, 25 avenue des Martyrs BP 166, Grenoble cedex 9, 38042 France*
[2]*CEA, INAC, SP2M Grenoble 38054 France*
[3]*A. M. Prokhorov General Physics Institute, Russian Academy of Sciences, 38 Vavilov street, Moscow 119991 Russia*
[4]*IPCMS, CNRS-UdS, 23 rue du Loess, F-67034 Strasbourg, France*
[5]*P. N. Lebedev Physical Institute, Russian Academy of Sciences, 53 avenue Leninskii, Moscow 119991 Russia*
(Dated: October 9, 2012)

X-ray absorption (XAS) and x-ray magnetic circular dichroism (XMCD) spectra at the $L_{2,3}$ edges of Mn in different (Ge,Mn) compounds are calculated from first principles. Early *ab initio* studies show that the Density Functional Theory (DFT) does not reproduce a characteristic change of sign in the L_3 XMCD spectrum of Mn in Ge_3Mn_5, which is observed in experiment. In this work we demonstrate that this disagreement is partially related to an underestimation of the exchange splitting of Mn $2p$ core states within the local density approximation. It is shown that the change in sign experimentally observed is reproduced if the exchange splitting is calculated within the Hartree-Fock approximation, while the final states can be still described by the DFT. This approach is further used to calculate the XMCD in different (Ge,Mn) compounds. It demonstrates the high sensitivity of XMCD, compared to XAS, to the local atomic structure around Mn absorbers.

PACS numbers: 75.50.Pp, 71.20.Lp, 78.70.Dm
Keywords: (Ge,Mn), XAS, XMCD

I. INTRODUCTION

The development of spintronics has emphasized the need for novel materials exhibiting a strong electric-magnetic interplay, as it would permit the design of new devices achieving an electric control of the magnetic properties, strongly spin-polarized currents and magneto-transport effects, or magneto-optical functions.

One class of such materials is that of diluted magnetic semiconductors (DMSs) presenting carrier induced ferromagnetism.[1] Magnetic impurities introduced in II-VI or III-V semiconductors exhibit a strong coupling to the carriers of the semiconductor, giving rise to giant magneto-optical (giant Zeman effect) and magneto-transport properties. If electrically doped, DMSs also feature ferromagnetic interactions[1] that depend on the carrier density in such a way[2] that the Curie temperature[3] and the magnetic anisotropy[4] can be controlled in field effect devices. It was rapidly recognized that in the quest for such materials, methods complementing magnetic studies were needed: the most widely used are magneto-optical spectroscopy (giant Zeeman effect and magnetic circular dichroism at the bandgap),[5] magneto-transport (magnetoresistance, anomalous Hall effect),[6] and x-ray spectroscopy (x-ray absorption spectroscopy, XAS, and x-ray magnetic circular dichroism, XMCD, at both K and L edges).

XAS and XMCD are two well established techniques for the study of the electronic and magnetic properties of materials. The existence of dichroism sum rules, which have been derived theoretically[7,8] and then successfully applied to XMCD experimental spectra,[9] makes it straightforward to extract quantitative information on the local spin and orbital magnetic moments, in particular in the case of the $L_{2,3}$ absorption edges of the transition metals. Several efficient ways of calculating the theoretical XAS and XMCD spectra from the electronic structure calculations are now available for both ionic and metallic systems, commonly based on the density functional theory (DFT). Both the sum rules and DFT calculations at the $L_{2,3}$ absorption edges work well for heavier $3d$ transition metals (*i.e.* Fe, Co), however they are more difficult to apply to lighter ones, such as Mn. A discrepancy as high as 50 to 80% or even a wrong sign has been reported between the value of the magnetic spin moment in $3d^4$ Mn^{3+} deduced from the application of the sum rule, and its expectation value (Note that for a $3d^5$ system the error is much reduced to a value between 68% and 74% with no wrong sign).[10] A difficulty in such an approach is that interaction between the photocreated $2p$-core hole and the $3d$-electrons of Mn modifies considerably the shape of $L_{2,3}$ spectra, leading to multiplet effects.[11] These effects are not always caught by DFT, and a disagreement between experimental and theoretical $L_{2,3}$ spectra is often found.

Unfortunately, Mn is the transition metal impurity which is the most widely used to make DMSs. In II-VI semiconductors such as selenides and tellurides, all compositions up to 100% Mn can be grown by molecular beam epitaxy. The most studied DMS with carrier induced ferromagnetism is (Ga,Mn)As where Mn substitutes Ga. Values of the Curie temperature have been improved but stay lower than 200 K. As this is too low for practical applications, and in order to ensure a good compatibility with silicon technology, some effort has been directed towards introducing Mn into Germanium. Recent reports have shown significantly higher Curie temperatures, but also that the distribution of magnetic impurity ions is inhomogeneous.[12–14] Such nanostructures, *e.g.* inclusions, contain a locally high concentration of Mn ions. Thus the observed high temperature ferromagnetism can be explained by a stronger exchange interaction between Mn ions, which are separated by shorter distances in the inclusion. Nevertheless, interesting magneto-transport properties have been reported. This class of hybrid systems[15] which exhibit high values of the Curie temperature and strong magneto-transport and/or magnetooptical properties, comprises also, *e.g.*, (Zn,Cr)Te,[16] (Ga,Mn)N and (Ga,Fe)N[17], and MnAs in GaAs,[18] to cite but a few examples.

Our main interest here is driven by understanding the electronic, magnetic and structural properties of self-assembled ferromagnetic (Ge,Mn) nanocolumns, a system in which high T_C (>400 K) have been reported.[19] The structural properties of the nanocolumns and surrounding Ge matrix have already been studied experimentally[20–23] and theoretically,[24,25] yet an experimental confirmation of the crystal phase in the nanocolumns is still to be obtained. Note that similarly high values of the Curie temperature have been found in other (Ge,Mn) samples with a different morphology.[26]

Turning to XAS and XMCD at the $L_{2,3}$ edges, the XAS line is generally broader than the XMCD one. In intermetallic compounds, it does not show the multiplet structure[27] which is usually present in oxides.[20] It is therefore difficult to use XAS to investigate the local atomic structure around absorbers.[28] XMCD spectra have a more developed structure and in this work they are used to study local atomic structure around Mn atoms in different compounds. However sum rules are difficult to use in the present case, first because the two components L_2 and L_3 overlap, and second because we deal with a non-homogeneous system. Also, the XMCD spectra measured in both (Ge,Mn) nanocolumns and in the metallic Ge_3Mn_5 alloy[28–30] (see Fig. 1 below) show a clear positive bump between the L_3 and L_2 lines. This signal could not be reproduced by DFT calculations so far.

This disagreement partially comes from an underestimation of the exchange splitting of Mn 2*p*-states within the local density approximation (LDA). Assuming that the exchange interaction between 2*p*- and 3*d*-electrons of Mn is weakly screened by valence electrons, we propose to evaluate the splitting within the Hartree-Fock (HF) approximation, whereas the valence states in metals are still calculated within DFT.

In this paper we apply this approach to increase the accuracy of the calculation of the XAS-XMCD spectra of Mn in the specific case of the ferromagnetic semiconductor (Ge,Mn) and related systems. This is done in a fashion that may be further applied to other systems.

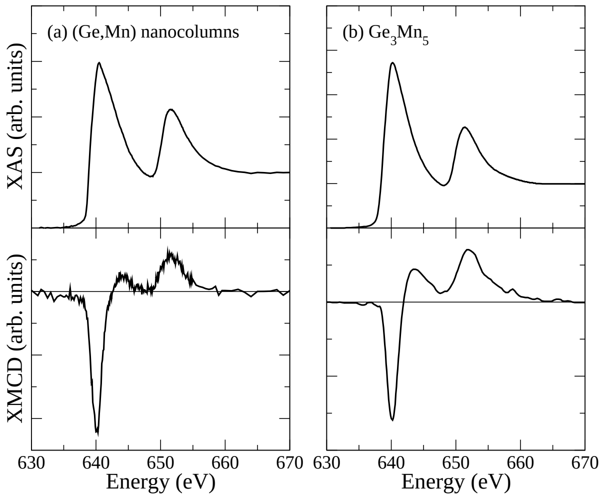

FIG. 1: (a) Experimental XAS and XMCD spectra in the (Ge,Mn) nanocolumns measured at a temperature of 5 K and in a 5 T magnetic field and (b) in Ge_3Mn_5 at 80 K and in remanence (from Ref. 30).

II. METHODS

Experimental spectra are available for (Ge,Mn) nanocolumn samples and for Ge_3Mn_5.

XAS and XMCD in (Ge,Mn) nanocolumn samples were carried out on thin films obtained by low-temperature molecular beam epitaxy. Details on the sample growth can be found in Ref. 23. The (Ge,Mn) samples were efficiently protected against oxidation by *in situ* deposition of a 3 nm-thick amorphous Si layer. Measurements were carried out at beamline UE46-PGM at the Helmholtz Center Berlin using the total electron yield method.[20] A magnetic field of 5 T has been applied in the plane of incidence of the x-rays to align the magnetization along the light propagation. The sample temperature was 5 K. Experimental XAS-XMCD spectra in the (Ge,Mn) nanocolumns system are shown in Fig. 1.

We also considered XAS-XMCD spectra of the ferromagnetic metal Ge_3Mn_5, as reported in the literature both for bulk single crystals[29] and for thin films,[28,30] see Fig. 1. They appear to be quite similar to those of the (Ge,Mn) nanocolumns.

Atomic calculations and *ab initio* DFT based methods are used to calculate XMCD spectra. *Ab initio* methods are based on an explicit band structure calculation, where hybridization of Mn atoms with neighbor atoms and related charge redistributions are taken into account. This method is therefore more suitable to predict XMCD spectra in compounds with different local atomic structure.

XAS spectra of (Ge,Mn) compounds have been computed from first principles using the FDMNES code.[32] In the dipole approximation, the x-ray absorption cross-section is given by:

$$\sigma(\omega) = 4\pi^2\alpha\hbar\omega \sum_{i,f} |< \phi_f|\hat{\epsilon}|\phi_i >|^2 \times\delta_\Gamma(\hbar\omega - \varepsilon_f + \varepsilon_i), \quad (1)$$

where α is the fine structure constant, ϕ_i, ε_i, and ϕ_f, ε_f are eigenfunctions and eigenvalues of the initial and final states correspondingly, δ_Γ is a Lorentzian curve of width Γ determined by the core-hole life-time, and $\hat{\epsilon_r}$ is the photon polarization. The absorption cross-section is calculated for the three orthogonal directions of light propagation (x,y,z), and the direction of the magnetization along the light propagation. Then a mean value of the cross-section is evaluated.

The electron final states in the cluster are calculated using the multiple-scattering approach and within the muffin-tin (MT) approximation.[33,34] The calculation is performed in a periodic crystal potential, but scattering paths are considered in a cluster with a diameter of 12 Å.

The crystal potential is obtained from a self-consistent solution of the Kohn-Sham equations within the general gradient approximation (GGA)[35] using the full-potential WIEN2k code.[36] The spherical part of the self-consistent crystal potential in each MT-sphere was retained for the XAS calculations. Then the Schrödinger (or Dirac) equation is solved in each MT-sphere.

The experimental lattice parameter of bulk Ge a=5.66 Å is used in all compounds, excepting Ge_2Mn(C16),[24] and Ge_3Mn_5. For the Ge_2Mn(C16) compound a=5.95 Å and c=5.03 Å parameters were obtained from a structural relaxation calculation,[24] while experimental values[37] a=7.184 Å and c=5.053 Å were used for Ge_3Mn_5. In all the structures atomic positions were relaxed, except for Ge_3Mn_5, where experimental atomic positions were taken from Ref. 37. Note that a previous calculation shows that a relaxation of internal atomic positions and lattice parameters within GGA does not change the experimental parameters.[38–40]

In most cases the Kohn-Sham eigenvalues and eigenfunctions, calculated in metals, are rather close to those obtained from the solution of the quasiparticle equation:

$$\left[-\frac{1}{2}\nabla^2 + V_{ext}(\mathbf{r}) + V_H(\mathbf{r})\right]\phi_{n\mathbf{k}}(\mathbf{r}) + \int \Sigma(\mathbf{r},\mathbf{r}',E_{n\mathbf{k}})\phi_{n\mathbf{k}}(\mathbf{r}')d\mathbf{r}' = E_{n\mathbf{k}}\phi_{n\mathbf{k}}(\mathbf{r}). \quad (2)$$

Therefore it is assumed that final state eigenfunctions ϕ_f and eigenvalues ε_f are well described by DFT in metallic compounds. Meanwhile the DFT eigenvalues of the initial states can be improved.

The initial states in x-ray absorption spectroscopy at the $L_{2,3}$ edges are the $2p$ core levels of Mn. They are split by the spin-orbit and $2p$-$3d$ exchange interactions, described by the ξ and H_{xc} parameters correspondingly. When H_{xc}=0, the $2p$ core levels are split into a $p_{3/2}$ and a $p_{1/2}$ states, separated by a $3\xi/2$ energy interval.[41] The spin-orbit splitting in a spherical atomic potential is given by the term:

$$\zeta(r)\mathbf{l}\cdot\mathbf{s},$$

where $\zeta(r) \sim \frac{1}{r}\frac{dV}{dr}$ and V is the atomic potential. This term is large for core orbitals, since they are localized near the atomic nucleus. The experimental spin-orbit splitting of the $2p_{3/2}$ and $2p_{1/2}$ orbitals is $3\xi/2$= 10.5 eV in Mn (ξ=7.0 eV).[42]

The exchange splitting H_{xc} of $2p_{j=3/2}^{m_j=3/2}$ and $2p_{j=3/2}^{m_j=-3/2}$ is smaller, $H_{xc}/\xi \ll 1$. This term arises from the exchange interaction between $2p$- and $3d$-electrons of the Mn atom. As a result,[41] the $2p$-level with j=3/2 is split into four successive sublevels (m_j=-3/2, -1/2, 1/2, 3/2) equally spaced by $H_{xc}/3$, with state m_j=3/2 being the lowest in energy. The $2p$-level with j=1/2 is split into two sublevels (m_j=1/2, -1/2), separated by $H_{xc}/3$, with sublevel m_j=-1/2 the lowest in energy. The exchange parameter H_{xc} can be evaluated as a difference between eigenvalues of the $2p$-core sublevels:

$$\mathrm{H}_{xc} = \epsilon_{j=3/2}^{m=-3/2} - \epsilon_{j=3/2}^{m=3/2}. \quad (3)$$

As the exchange interaction between the $2p$- and $3d$-electrons of a Mn atom is weakly screened by valence electrons, a good estimate of the value of the exchange splitting H_{xc} can be obtained within the Hartree-Fock approximation, from a calculation of the exchange term in the self-energy:

$$\mathrm{H}_{xc} =< \phi_{j=3/2}^{m=-3/2}|Gv|\phi_{j=3/2}^{m=-3/2} > - < \phi_{j=3/2}^{m=+3/2}|Gv|\phi_{j=3/2}^{m=+3/2} >, \quad (4)$$

where the Green's function is composed by the $3d$-orbitals of the Mn atom, v is the bare Coulomb potential, and ϕ_j^m are $2p$-core orbitals of the same Mn atom, calculated by the DFT method. It is expected that the contribution of other terms of the quasiparticle equation (2) is smaller since the radial parts of ϕ_j^m orbitals with j=3/2,m_j=-3/2 and j=3/2,m_j=+3/2 are almost identical.

In most cases, the spin-orbit interaction between valence electrons is neglected in our calculation (*i.e.*, the Schrödinger equation is solved in each MT-sphere) whereas the spin-orbit splitting of the $2p$ core states is always taken into account. In order to evaluate the effect of spin-orbit interaction between valence electrons on absorption spectra, fully relativistic calculations of final states in Eq. (1) were also performed.

The XAS and XMCD signals are evaluated as $(\sigma^+ + \sigma^-)/2$ and $(\sigma^+ - \sigma^-)$, respectively, where σ^+ and σ^- are absorption cross-sections for the two circular polarizations of x-ray radiation.

Calculated XAS and XMCD spectrum at the $L_{2,3}$-edges of Mn were convoluted with a Lorentzian function

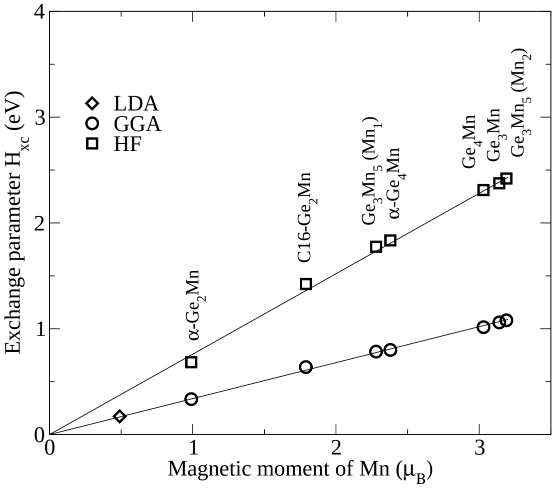

FIG. 2: Exchange splitting of Mn 2*p*-states in different compounds (see text), calculated within the GGA (circles) and the HF approximation (squares). Numerical values are given in Tab. I. The diamond symbols corresponds to the α-Ge$_2$Mn compound calculated within the LDA.

to account for the core hole lifetime (for the sake simplicity the same value 0.32 *eV* was used for both the L$_2$ and L$_3$-edges). A complementary convolution with a Gaussian function to account for the experimental resolution and scaling of the spectra was performed to compare the calculated spectra with the experimental ones. Typical broadening parameters $\sigma = 1.0$ *eV* and $\sigma = 0.5$ *eV* (where σ is the standard deviation of the Gaussian function) were used[38]. The smaller value was used for the XMCD spectra so as not to completely wash out the structure of the peaks that will be discussed hereafter.

III. RESULTS

A. Exchange splitting of 2*p*-core levels

The exchange splitting H_{xc} in different compounds (these compounds are described in more details in the next sections) was calculated within the GGA and the HF approximation. Calculation parameters and corresponding exchange splitting values are listed in Table I. H_{xc} is plotted as a function of Mn spin moment in Fig. 2.

The dependence of the exchange splitting H_{xc} on Mn spin moment is almost linear, and actually small deviations from the linearity can be related to different radii of MT-spheres which were used to compute Mn spin moments in the different compounds.

The value of H_{xc} is greatly underestimated within LDA and GGA. This shows the inadequacy of both LDA and GGA to describe correctly such an effect. Note that within the LDA (illustrated only for the α-Ge$_2$Mn compound in Fig. 2 for clarity), not only the exchange splitting but also the magnetic moment on the Mn atom are underestimated.

B. Ge$_3$Mn$_5$, a test material

As mentioned earlier, the intermetallic compound Ge$_3$Mn$_5$ displays experimental XAS-XMCD spectra similar to those observed in the (Ge,Mn) nanocolums (Fig. 1). Accordingly, we start our detailed study by considering this well-known system, which is available in bulk form and as thin epitaxial layers. It has a hexagonal crystal structure with a space group P6$_3$/*mcm* and lattice parameters a=7.184 Å and c=5.053 Å.[37] The primitive cell contains three inequivalent atoms, Mn$_1$, Mn$_2$ and Ge, in positions:[38]

4(d) Mn$_1$:$\pm(\frac{1}{3},\frac{2}{3},0)$,$\pm(\frac{2}{3},\frac{1}{3},\frac{1}{2})$

6(g) Mn$_2$:$\pm(x,0,\frac{1}{4})$,$\pm(0,x,\frac{1}{4})$,$\pm(-x,-x,\frac{1}{4})$, x=0.2397

6(g) Ge:$\pm(x,0,\frac{1}{4})$, $\pm(0,x,\frac{1}{4})$, $\pm(-x,-x,\frac{1}{4})$, x=0.6030

The experimental magnetic spin moments of Mn$_1$ and Mn$_2$ atoms are different: 1.96(3) μ_B and 3.23(2) μ_B correspondingly (calculated values are listed in Table I). This difference was attributed to different atomic structures around the Mn atoms.[37] The local atomic structure of Mn atoms in Ge$_3$Mn$_5$, as given in Ref. 37, is the following: (*i*) Mn$_1$ neighbors are two Mn$_1$, six Ge and six Mn$_2$ at distances 2.522 Å, 2.534 Å and 3.059 Å respectively; (*ii*) Mn$_2$ neighbors are two Mn$_2$, four Mn$_2$ and four Mn$_1$ at distances 2.976 Å, 3.051 Å and 3.059 Å respectively. The two Mn atoms nearest-neighbors to Mn$_1$ atoms are at a short distance (2.522 Å) and it was suggested that the interaction with these neighbors would lead to a reduction of the magnetic spin moment of Mn$_1$ atoms. The calculated total spin moment per Mn atom is 2.75 μ_B, in agreement with previous calculations.[38,39] This value is slightly higher than the experimental one, *i.e.* 2.60 μ_B.[37] It was shown that a good agreement with experiment is found within GGA and including the spin-orbit interaction into the calculation.[38]

The partial density of 3*d*-states of Mn in Ge$_3$Mn$_5$ is shown in Fig. 3. It is interesting to compare it with the Mn 3*d* DOS in a diluted magnetic semiconductor Ga$_{1-x}$Mn$_x$As (x=0.125), where Mn atoms substitute Ga. The density of states at the Fermi level in Ge$_3$Mn$_5$ is significant in both spin channels and this compound has a metallic conductivity, as it was found in previous calculations.[38]

Because of a strong interaction between Mn atoms, the 3*d*-bands in Ge$_3$Mn$_5$ are broad. The L$_{2,3}$ spectra reflect electron transitions from the narrow 2*p*- into the broad valence 3*d*-bands of Mn, hence the lineshapes in XMCD spectra at the L$_{2,3}$ edges of Mn in intermetallic compounds is determined by the width of the valence bands.

It can be seen from Fig. 3, that the L$_2$ and L$_3$ edges are narrow in Ga$_{1-x}$Mn$_x$As (x=0.125), in agreement with the narrow bands calculated for this DMS.

TABLE I: Values of structural and magnetic parameters obtained from an *ab initio* calculation: R_{MT} is the radius of a muffin-tin sphere around the atom; M_{local} is the magnetic spin moment of the atom, calculated by integration of the spin density over the sphere; M_{TOT} is the magnetic spin moment per formula unit; H_{xc} is the splitting parameter, introduced in Eq. 4. For each compound, the number of atoms of each sort is indicated by the multiplication factor.

	Ge_3Mn_5			Ge_2Mn-α		Ge_4Mn-α		Ge_2Mn-C16		Ge_3Mn			Ge_4Mn			
	2×Mn_1	3×Mn_2	3×Ge_1	1×Mn_1	2×Ge_1	1×Mn_1	4×Ge_1	1×Mn_1	2×Ge_1	1×Mn_1	1×Ge_1	2×Ge_2	1×Mn_1	1×Ge_1	1×Ge_2	2×Ge_3
R_{MT}, Å	1.241	1.241	1.241	1.254	1.254	1.281	1.281	1.201	1.249	1.185	1.138	1.138	1.185	1.138	1.138	1.138
M_{local}, μ_B	2.28	3.19	-0.15	1.00	-0.02	2.38	-0.04	1.79	-0.08	3.14	0.03	-0.13	3.03	0.00	0.02	-0.01
M_{TOT}, μ_B	13.73			0.96		2.19		1.58		2.98			3.16			
H_{xc}, eV	1.775	2.420		0.684		1.835		1.423		2.375			2.311			

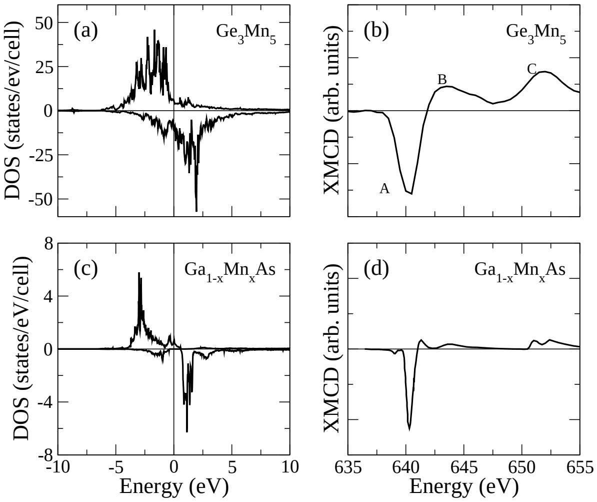

FIG. 3: $3d$-states of Mn in (a) Ge_3Mn_5 and (c) $Ga_{1-x}Mn_xAs$ (x=0.125). Experimental XMCD spectra at the $L_{2,3}$ edges of Mn in (b) Ge_3Mn_5 (from Ref. 30) and (d) $Ga_{1-x}Mn_xAs$ (x=0.084, from Ref. 31).

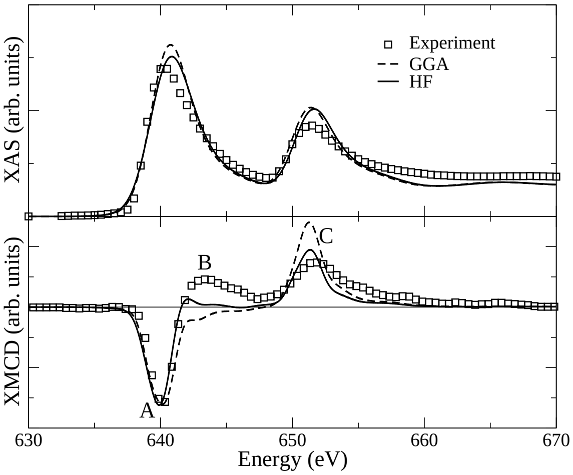

FIG. 4: Calculated (a) XAS and (b) XMCD spectra of Ge_3Mn_5 at the $L_{2,3}$-edges of Mn. The exchange splitting of the Mn $2p$ core levels was evaluated within GGA (dash line) and HF approximation (solid line). Experimental data were taken from Ref. 30.

The resulting XAS and XMCD spectrum, calculated within GGA and HF approximation, are shown in Fig. 4. XAS obtained within both approximations are similar and contain L_2 and L_3 edges without visible multiplet structure. A large value of the convolution parameter $\sigma = 1\ eV$ in Gaussian functions allows us to reproduce the broad absorption lines found in experimental $L_{2,3}$ spectra of Mn.

The XMCD spectrum contains a fine structure, which can be used to distinguish compounds with different atomic structure around Mn atoms. When all the $3d$-states with spin up are occupied, the XMCD spectrum shows a negative A peak and a positive C peak.[43] In solids, the $3d$ states of Mn are partially occupied and the XMCD spectrum has a more complicated structure: the main absorption line A in the L_3 edges is followed by a positive peak B (Fig. 3). This feature of the absorption line is not reproduced by the DFT-GGA calculation,[28,38] however a description of Mn $2p$-$3d$ exchange interaction within the HF approximation allows us to obtain a qualitative agreement with experiment. In particular, line B is reproduced, although its intensity is smaller than in experiment (Fig. 4). The intensity ratio between the two absorption edges L_2 and L_3 is improved as well.

The influence of spin-orbit interaction on the absorption spectrum was studied by solving the Dirac equation for the initial and final states. Then the exchange splitting of Mn $2p$ sublevels was corrected and the absorption spectrum was calculated according to Eq. (1). The influence of spin-orbit interaction on XAS and XMCD spectrum was found to be small (Fig. 5), and essentially the same spectrum is obtained by solving the Shrödinger equation with spin polarization in MT-spheres.

C. The α-Ge_2Mn structure

Another structure was initially proposed by Takizawa *et al.*[44] for Ge_4Mn, and further discussed by Arras *et al.*[25] for α-Ge_2Mn as a likely candidate for the crystalline structure of the nanocolumns in (Ge,Mn) layers. This structure is derived from cubic Ge, in which the presence of interstitial Mn atoms lowers the formation energy. The formation energy of the α-Ge_2Mn was also found to be lower than that of Ge with the usual diamond

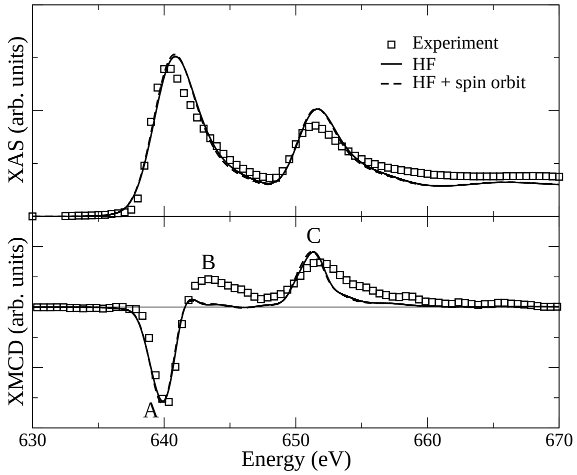

FIG. 5: Calculated (a) XAS and (b) XMCD spectra of Ge_3Mn_5 at the $L_{2,3}$-edges of Mn with (dashed line) and without (solid line) spin-orbit interaction. Both spectra are almost superimposed, showing the small influence of the spin-orbit interaction in this metallic compound. The exchange splitting of Mn $2p$ core levels was evaluated within HF approximation.

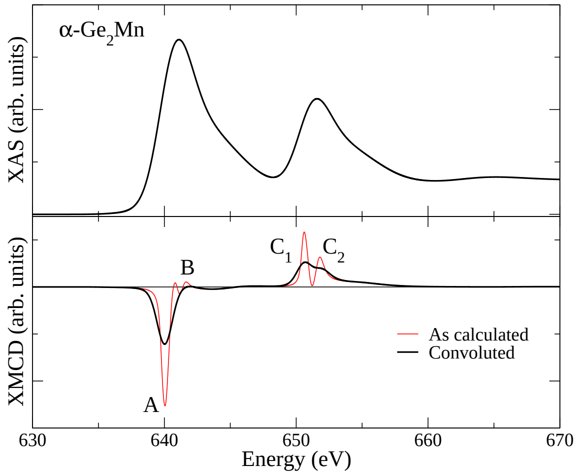

FIG. 6: Calculated (a) XAS and (b) XMCD spectra of α-Ge_2Mn at the $L_{2,3}$-edges of Mn. The calculated XMCD spectrum is shown by a thin red line. The same spectrum after convolution with the Lorentzian and Gaussian functions is shown by a thick line. The exchange splitting of Mn $2p$ core levels was evaluated within the HF approximation.

structure containing the same amount of substitutional and interstitial Mn. This phase is all the more favorable when the concentration of substitutional or interstitial Mn increases.[25]

The XAS and XMCD spectra of α-Ge_2Mn were calculated and convoluted with Lorentzian and Gaussian functions in the same manner as it was done for Ge_3Mn_5. The resulting spectra are shown in Fig. 6. As in the case of Ge_3Mn_5, it is predicted that XAS of α-Ge_2Mn has no fine structure so that it can hardly be used to study the local atomic environment of Mn.

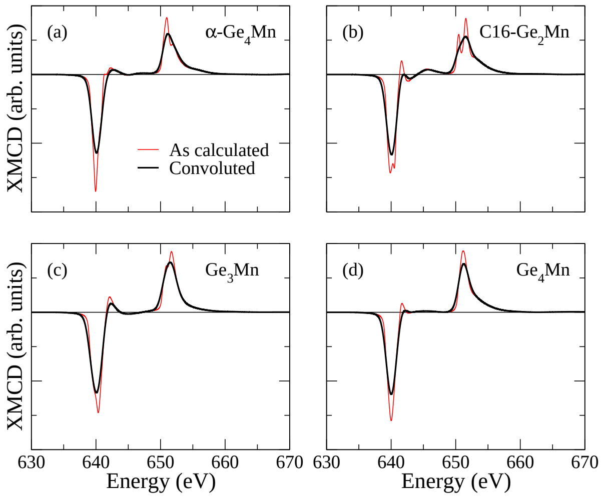

FIG. 7: Calculated XMCD spectra at the $L_{2,3}$-edges of Mn in different (Ge,Mn) compounds (a) α-Ge_4Mn, (b) C16-Ge_4Mn, (c) Ge_3Mn with substitutional Mn in Ge with diamond structure and (d) Ge_4Mn with interstitial Mn in Ge with the diamond structure. The calculated XMCD spectrum is shown by a thin red line. The same spectrum after convolution with the Lorentzian and Gaussian functions is shown by a thick black line. The exchange splitting of Mn $2p$ core levels was evaluated within the HF approximation.

In contrast, the XMCD spectrum has a more detailed structure (Fig. 6), and for this reason only XMCD spectra will be further considered. The $L_{2,3}$ XMCD spectrum of Mn contains a negative line A, followed by a slightly negative broad line B in the L_3 edge. The positive line C at the L_2 edge is not symmetric: its left side is sharper that the right one. This asymmetry is due to a splitting of the line C into a more intense C_1 and a less intense C_2 lines.

The positive line B, observed in the XMCD spectrum of Ge_3Mn_5, is absent in the spectrum of α-Ge_2Mn. The local magnetic moment of Mn in this structure is low ($1\mu_B$), and the exchange splitting of Mn $2p$-states is small. As it was shown in previous section, the line B is reproduced in calculated spectra of Mn if the exchange splitting is properly evaluated, *i.e.*, if the splitting of $2p$-states underestimated within GGA, is increased approximately by a factor 2. This suggests that an increase of the local spin moment of Mn, together with the corresponding increase of the exchange splitting, would lead to the appearance of the line B in the XMCD spectrum of α-Ge_2Mn.

As a matter of fact, such an increase of the local spin moment of Mn is expected if vacancies are created at the Mn positions in α-Ge_2Mn. In particular, in a α-Ge_4Mn phase which has the crystal structure of α-Ge_2Mn, but only 50% of Mn atoms in their original positions, the local spin moment of Mn is increased to 2.4 μ_B (Tab. I). Then line B appears in the theoretical XMCD spectrum (Fig. 7a).

D. The C16-Ge$_2$Mn structure

A Ge$_2$Mn phase, related to the α-phases, was proposed in Ref. 24. This phase has a tetragonal lattice structure with a cell volume smaller than the one in bulk Ge. The calculated spin moment of Mn in C16-Ge$_2$Mn is 1.8 μ_B, that is, larger than the Mn spin moment in α-Ge$_2$Mn (1.0 μ_B). This increased value of the Mn spin moment enhances the exchange splitting of the $2p$-core states (Fig. 2).

Different band structures in the α- and C16-phases, as well as different values of the $2p$-levels exchange splitting, cause differences in their XMCD spectra. The line B in the XMCD spectrum of C16-Ge$_2$Mn contains a negative part, which is followed by a positive one (Fig. 7b). This unusual behavior of the B line may be used to identify the C16-Ge$_2$Mn phase.

E. Ge$_3$Mn and Ge$_4$Mn with diamond structure

We now consider Ge with the usual diamond structure, where Mn atoms are located in substitutional or interstitial positions. The Mn concentrations were taken to be 25% for substitutional Mn (*i.e.*, Ge$_3$Mn) and 20% for interstitial Mn (*i.e.*, Ge$_4$Mn). These compositions are within the range experimentally observed in different Mn-rich (Ge,Mn) phases, 15%-40%.[19,23,45]

The calculated XMCD spectra of both substitutional and interstitial Mn in Ge (Fig. 7 c,d) are quite close. In Ge$_3$Mn with substitutional Mn, the intensity of line C is larger than in other phases. In Ge$_4$Mn with interstitial Mn, line B is weaker, in spite of a large local spin moment on Mn and the related large exchange splitting of $2p$-states (Tab. I). Also line C is narrower than in other compounds.

F. Discussion

Many-body effects, such as relaxation of the electron system after excitation,[46] and the mixing of L$_2$ and L$_3$ edges due to Coulomb interaction between electrons of Mn,[47] are not taken into account in this calculation and may modify the XMCD spectrum. In addition, the influence of defects on the electronic state of Mn should be also taken into account when a comparison to experimental spectra is done, as well as the disordered structures in the nanocolumn samples, which contain Mn in the nanocolumns but also in the matrix and at the interface. All these factors make it difficult to use XMCD spectra for the determination of the crystal structures of metallic compounds. However, the more accurate calculation of the XMCD spectra using the precise calculation of the eigenvalues of the initial $2p$-states within the Hartree-Fock approximation reveals details on the XMCD spectra lineshape (*e.g.* the presence or absence of the positive peak labeled B at about 643 eV) that were up to now eluded in standard calculations.

IV. SUMMARY AND CONCLUSIONS

XAS and XMCD spectra at the L$_{2,3}$ edges of Mn in different (Ge,Mn) compounds were calculated from first principles. Early calculations show that DFT-based calculations are not able to reproduce some features in the XMCD spectra of Mn. In particular, the positive part of the L$_3$ edges of Mn in Ge$_3$Mn$_5$ is absent in the calculated XMCD spectrum, while it is observed in experiment. In this work we show that this positive part can be reproduced if the eigenvalues of initial $2p$-states are calculated within HF approximation. The final valence states can be still described within DFT, since the DFT eigenvalues in metals are rather close to quasiparticle energies. The effect of spin-orbit interaction between valence electrons was also considered and found to be small.

(Ge,Mn) compounds with a large content usually feature a metallic character. The XAS of such metallic compounds are broad and have no particularities which can help to identify different compounds. XMCD spectra have a more detailed structure and their shape depends on the local spin moment of Mn and the crystal structure. In this work we compare XMCD spectra calculated for two energetically stable phases of (Ge,Mn), with those calculated for substitutional and interstitial Mn in Ge. The XMCD spectra of all the (Ge,Mn) phases have a similar structure and shape, but also small peculiar features which can be used to identify a particular (Ge,Mn) compound.

Acknowledgments

Authors acknowledge financial support from the French Research Agency (project ANR GEMO), the Grenoble Nanosciences Foundation, the Russian Fund for Basic Research (RFBR No 10-02-00698) and the Russian Ministry of Education and Science. Calculations were performed at the CIMENT supercomputer center via the NanoSTAR project. We also gratefully acknowledge the assistance of Detlef Schmitz during experiments at beamline UE46-PGM, Helmholtz Center, Berlin.

---

[*] current affiliation: RIKEN, SPring-8 Center, Sayo, Hyogo 679-5198, Japan; samuel.tardif@spring8.or.jp

[†] pascal.pochet@cea.fr

[1] H. Ohno, Science **281**, 951 (1998).

[2] T. Dietl, H. Ohno, F. Matsukura, J. Cibert, D. Ferrand, Science **287**, 1019 (2000).

[3] D. Chiba, M. Yamanouchi, F. Matsukura, H. Ohno, Science **301** 943 (2003).

[4] D. Chiba, M. Sawicki, Y. Nishitani, Y. Nakatani, F. Matsukura and H. Ohno, Nature **455**, 515 (2008).

[5] K. Ando, Science **312**, 1883 (2006).

[6] T. Jungwirth, Qian Niu, and A. H. MacDonald, Phys. Rev. Lett. **88**, 207208 (2002).

[7] B. T. Thole, P. Carra, F. Sette, and G. van der Laan, Phys. Rev. Lett. **68**, 1943 (1992).

[8] P. Carra, B. T. Thole, M. Altarelli, and X. Wang, Phys. Rev. Lett. **70**, 694 (1993).

[9] C. T. Chen, Y. U. Idzerda, H.-J. Lin, N. V. Smith, G. Meigs, E. Chaban, G. H. Ho, E. Pellegrin, and F. Sette, Phys. Rev. Lett. **75**, 152 (1995).

[10] C. Piamonteze, M. Piter, and F. M. F. de Groot, Phys. Rev. B **80**, 184410 (2009).

[11] F. de Groot and A. Kotani, "Core level spectroscopy of solids", CRC Press (2008).

[12] X. Chen, M. Na, M. Cheon, S. Wang, H. Luo, B. D. McCombe, X. Liu, Y. Sasaki, T. Wojtowicz, J. K. Furdyna, S. J. Potashnik, and P. Schiffer, Appl. Phys. Lett. **81**, 511 (2002).

[13] M. Moreno, A. Trampert, B. Jenichen, L. Däweritz, and K. H. Ploog, J. Appl. Phys. **92**, 4672 (2002).

[14] A. P. Li, J. F. Wendelken, J. Shen, L. C. Feldman, J. R. Thompson, H. H. Weitering, Phys. Rev. B **72**, 195205 (2005).

[15] T. Dietl, Nat. Mater. **9**, 965 (2010).

[16] S. Kuroda, N. Nisizawa, K. Takita, M. Mitome, Y. Bando, K. Osuch, and T. Dietl, Nature Mat. **6**, 440 (2007).

[17] A. Bonanni, A. Navarro-Quezada, Tian Li, M. Wegscheider, Z. Matěj, V. Holý, R. T. Lechner, G. Bauer, M. Rovezzi, F. D'Acapito, M. Kiecana, M. Sawicki, and T. Dietl, Phys. Rev. Lett. **101**, 135502 (2008).

[18] P. N. Hai, S. Ohya, M. Tanaka, S. E. Barnes, and S. Maekawa, Nature **458**, 489 (2009).

[19] M. Jamet, A. Barski, T. Devillers, V. Poydenot, R. Dujardin, P. Bayle-Guillemaud, J. Rothman, E. Bellet-Amalric, A. Marty, J. Cibert, R. Mattana, and S. Tatarenko, Nat. Mater. **5**, 653 (2006).

[20] S. Tardif, S. Cherifi, M. Jamet, T. Devillers, A. Barski, D. Schmitz, N. Darowski, P. Thakur, J. C. Cezar, N. B. Brookes, R. Mattana, and J. Cibert, Appl. Phys. Lett. **97**, 062501 (2010).

[21] S. Tardif, V. Favre-Nicolin, F. Lançon, E. Arras, M. Jamet, A. Barski, C. Porret, P. Bayle-Guillemaud, P. Pochet, T. Devillers, and M. Rovezzi, Phys. Rev. B **82**, 104101 (2010).

[22] M. Rovezzi, T. Devillers, E. Arras, F. d'Acapito, A. Barski, M. Jamet, and P. Pochet, Appl. Phys. Lett. **92**, 242510 (2008).

[23] T. Devillers, M. Jamet, A. Barski, V. Poydenot, P. Bayle-Guillemaud, E. Bellet-Amalric, S. Cherifi, and J. Cibert, Phys. Rev. B **76**, 205306 (2007).

[24] E. Arras, I. Slipukhina, M. Torrent, D. Caliste, T. Deutsch, and P. Pochet, Appl. Phys. Lett. **96**, 231904 (2010).

[25] E. Arras, F. Lançon, I. Slipukhina, E. Prestat, M. Rovezzi, S. Tardif, A. Titov, P. Bayle-Guillemaud, F. d'Acapito, A. Barski, V. Favre-Nicolin, M. Jamet, J. Cibert, and P. Pochet Phys. Rev. B **85**, 115204 (2012).

[26] F. Xiu, Y. Wang, J. Kim, A. Hong, J. Tang, A. P. Jacob, J. Zou, and K. L. Wang, Nat. Mater. **9**, 337 (2010).

[27] A. Kimura, S. Suga, T. Shishidou, S. Imada, T. Muro, S. Y. Park, T. Miyahara, T. Kanenko, T. Kanomata, Phys. Rev. B. **56**, 6021 (1997).

[28] L. Sangaletti, G. Drera, E. Magnano, F. Bondino, C. Cepek, A. Sepe, and A. Goldoni, Phys. Rev. B **81**, 085204 (2010).

[29] C. Hirai, H. Sato, A. Kimura, K. Yaji, K. Iori, M. Taniguchi, K. Hiraoka, T. Muro and A. Tanaka, Physica B: Condensed Matter **351**, 341 (2004).

[30] P. De Padova, J.-P. Ayoub, I. Berbezier, P. Perfetti, C. Quaresima, A. M. Testa, D. Fiorani, B. Olivieri, J.-M. Mariot, A. Taleb-Ibrahimi, M. C. Richter, O. Heckmann, and K. Hricovini, Phys. Rev. B **77**, 045203 (2008).

[31] K. W. Edmonds, G. van der Laan, A. A. Freeman, N. R. S. Farley, T. K. Johal, R. P. Campion, C. T. Foxon, B. L. Gallagher, and E. Arenholz, Phys. Rev. Lett. **96**, 117207 (2006).

[32] Y. Joly, Phys. Rev. B **63**, 125120 (2001); Y. Joly, S. Di Matteo, and C. R. Natoli, Phys. Rev. B **69**, 224401 (2004); O. Bunău and Y. Joly, J. Phys.: Condens. Matter **21**, 345501 (2009).

[33] C. R. Natoly, M. Benfatto, and S. Doniach, Phys. Rev. A **34**, 4682 (1986).

[34] S. I. Zabinsky, J. J. Rehr, A. Ankudinov, R. C. Albers, M. J. Eller, Phys. Rev. B **52**, 2995 (1995).

[35] J. P. Perdew, K. Burke, and M. Ernzerhof, Phys. Rev. Lett. **77**, 3865 (1996).

[36] P. Blaha, K. Schwarz, G. K. H. Madsen, D. Kvasnicka and J. Luitz, WIEN2k, An Augmented Plane Wave + Local Orbitals Program for Calculating Crystal Properties (Karlheinz Schwarz, Techn. Universität Wien, Austria), 2001. ISBN 3-9501031-1-2

[37] J. B. Forsyth and P. J. Brown, J. Phys.: Condens. Matter **2**, 2713 (1990).

[38] S. Picozzi, A. Continenza, and A. J. Freeman, Phys. Rev. B. **70**, 235205 (2004).

[39] I. Slipukhina, E. Arras, Ph. Mavropoulos, and P. Pochet, Appl. Phys. Lett. **94**, 192505 (2009).

[40] E. Arras, D. Caliste, T. Deutsch, F. Lancon, and P. Pochet, Phys. Rev. B **83**, 174103 (2011)

[41] G. van der Laan, Phys. Rev. B **51**, 240 (1995).

[42] Y. Ishiwata, M. Watanabe, R. Eguchi, T. Takeuchi, Y. Harada, A. Chainani, S. Shin, T. Hayashi, Y. Hashimoto, S. Katsumoto, and Y. Iye, Phys. Rev. B **65**, 233201 (2002).

[43] G. van der Laan, C. M. B. Henderson, R. A. D. Pattrick, S. S. Dhesi, P. F. Schofield, E. Dudzik, D. J. Vaughan, Phys. Rev. B **59**, 4314 (1999).

[44] H. Takizawa, T. Sato, T. Endo, and M. Shimada, J. Solid State Chem. **88**, 384 (1990).

[45] D. Bougeard, S. Ahlers, A. Trampert, N. Sircar, and G. Abstreiter, Phys. Rev. Lett. **97**, 237202 (2006).

[46] J. J. Rehr, J. A. Soininen, and E. L. Shirley, Phys. Scr. **T115**, 207 (2005).

[47] Y. Teramura, A. Tanaka, and T. Jo, J. Phys. Soc. Jap. **65**, 1053 (1996).